Supporting Information for

The interplay between liquid-liquid and ferroelectric phase transitions in supercooled water

Maria Grazia Izzo, John Russo, Giorgio Pastore

Corresponding Author Maria Grazia Izzo
E-mails: mariagrazia.izzo@unive.it; mariagraziaizzo@gmail.com

This PDF file includes:

Supporting text
Figs. S1 to S13
SI References

Supporting Information Text

I. Temporal evolution of density and polarization in MD simulations in the (p, T) plane. In Figs. S1-S3 it is depicted the temporal evolution of P, P_i, and ρ obtained from extensive MD simulations of TIP4P/Ice water lasting up to 40 μs of Ref. (1) in several points of the (p, T) plane: along the line p = 1000 bar and p = 0 bar for different T's, crossing the Widom line (WL), and along the line p = 2500 bar for different T's, crossing the first-order liquid-liquid phase transition (LLPT) line.

II. Spatial distribution of dipoles in LDL and HDL configurations.. Although the results presented in this study are based on the establishment of a non-zero total spontaneous polarization in LDL, independently of the specific underlying local dipole order, it is still valuable to scrutinize the dipole configuration in LDL, particularly in comparison to HDL. The spatial distribution of single-molecule dipoles, $\mathbf{d}_i$, in instantaneous MD simulation configurations of LDL and HDL is shown in Figs. S4 and S5, respectively. The instantaneous polarization magnitude, $P(t)$, can be non-zero in HDL as well, due to large polarization fluctuations. We deliberately select an HDL configuration with a non-zero value of $P(t)$ to examine whether the instantaneous local distribution of dipoles generating a non-zero $P(t)$ in HDL differs from that in LDL. Although at first glance, *Panel a* of Figs. S4 and S5 suggests a higher degree of disorder in the spatial distribution of dipoles in LDL compared to HDL, distinguishing between a disordered state and one with a more complex underlying order remains challenging. Better insight can be gained by examining *Panel c* of Figs. S4 and S5, where it is shown the spatial distribution of dipoles $\mathbf{D}_i = \sum_{j\in L_i^3} \mathbf{d}_j$, where the simulation box is evenly divided into cells of size $L_i = L/3$, with L being the simulation box size. In particular, *Panel c-III* and *c-IV*, which display the projection of $\mathbf{D}_i$ onto a plane orthogonal to $\mathbf{P}(t)$, reveal distinct spatial distributions of dipoles in HDL and LDL. In HDL, despite the appearance of a preferential orientation of dipoles, their direction appears disordered. Conversely, in LDL, there seems to be a directional order reminiscent of a chiral distribution. Although these observations are not conclusive and a detailed analysis is beyond the scope of this manuscript, it would be interesting to explore the presence of local dipolar chiral order in LDL, consistent with the observation of local molecular chiral order reported in Ref. (2). Suitable order parameters and supervised machine learning methods could be exploited.

III. Non-local static correlation functions in supercooled water. Fig. S6 shows the $\mathbf{k}$-dependent transverse and longitudinal (to $\mathbf{k}$) static dielectric functions, respectively $\epsilon_{T\hat{k}}(k)$ and $\epsilon_{L\hat{k}}(k)$ and the static structure factor $S(k)$ in the HDL, LDL and close to CP. Since $S(k \to 0) = \rho K_B T K_T$, at CP, $S(k \to 0)$ should diverge. In Fig. S6 it is observed a gradual rise in $S(k)$ for small k's at the thermodynamic point close to CP. A more pronounced increase, indicative of a divergence as $k \to 0$, is observed at a k-scale smaller than what is attainable in the current MD simulations with $N = 1000$ (1). For $k \neq 0$, $\epsilon_T(k)$ holds only the physical meaning of a static correlation function, preserving $\epsilon_T(k) - 1$ the quality of a response function only in the limit $k \to 0$, while $\chi_L(k) = 1/(1 - \epsilon_L(k))$ is a static response function (3). This implies that for a thermodynamically stable system, $\epsilon_L(k) \geq 1$ or $\epsilon_L(k) < 0$ (3, 4). Additionally, a divergence occurs when $\epsilon_L = 1$, as observed in Fig. S6. Another divergence has been detected at higher k values under ambient conditions (4), ensuring that the correct physical limit, $\lim_{k\to\infty} \epsilon_L(k) = 1$, is reached (4).

IV. Mean field DFT for polar liquids with polarizable molecules. The following note is not intended to provide an exhaustive treatment of the generalization of DFT from non-polarizable, as presented in the main text, to polarizable molecules. Instead, it aims to demonstrate that introducing molecular polarizability in the polar liquid does not qualitatively change the results obtained for non-polarizable molecules.

Suppose that the single molecules in the liquid exhibit a mean electric dipole moment in response to a local field, which, in the absence of an external electric field, is proportional to $\boldsymbol{\delta}$. The single-molecule dipole thus becomes

$$\boldsymbol{d}(\delta) = \boldsymbol{d} + \alpha\boldsymbol{\delta}, \tag{1}$$

where $\boldsymbol{d}$ is the dipole molecule when $\delta = 0$ and α is a positive coefficient proportional to the molecular polarizability. The change in the molecular dipole, as given in Eq. 1, corresponds to substituting the ansatz for $\zeta(\Omega)$ in Eq. 2 of the main text with the following expression

$$\zeta(\Omega) = \frac{1 + \boldsymbol{\delta}(1 + \alpha\delta/d)\hat{d}}{4\pi}. \tag{2}$$

A full treatment would proceed self-consistently, where the increased total polarization of the liquid, generated by the larger molecular dipole in Eq. 1, would in turn generate a larger induced molecular dipole, and so forth. This iterative process would introduce higher-order terms in δ powers into the free energy expression. However, since our focus is on the lower-order terms in the free energy, we limit our analysis to the first step of the self-consistent procedure, which is equivalent to using the ansatz in Eq. 2. By applying the ansatz in Eq. 2 to the expressions of F_0 and $\mathcal{F}$ in Eqs. 24-26 of the main text, and performing a δ-series expansion of F_0 along with a ρ-Taylor expansion of both F_0 and $\mathcal{F}$, in place of Eqs. 29 and 30 in the main text, we obtain

$$F_0 = N\phi_0(\bar{\rho}) + MN\Delta\rho^2 + TN[A\delta^2 + 2A\frac{\alpha}{d}\delta^3 + (B + A\frac{\alpha^2}{d^2})\delta^4 + 4B\frac{\alpha}{d}\delta^5 + (B' + 6B\frac{\alpha^2}{d^2})\delta^6 + o(\delta^6)] \tag{3}$$

$$\mathcal{F} = -N\beta_0(\bar{\rho})\bar{\rho}\delta^2 + N\beta_1(\bar{\rho})\bar{\rho}\delta^2\Delta\rho - 2N\beta_0(\bar{\rho})\bar{\rho}\frac{\alpha}{d}\delta^3 + 2N\beta_1(\bar{\rho})\bar{\rho}\frac{\alpha}{d}\delta^3\Delta\rho - N\beta_0(\bar{\rho})\bar{\rho}\frac{\alpha^2}{d^2}\delta^4 + N\beta_1(\bar{\rho})\bar{\rho}\frac{\alpha^2}{d^2}\delta^4\Delta\rho. \tag{4}$$

Consequently Eq. 24 in the main text is substituted by

$$F = \phi_0(\bar{\rho}) + M\Delta\rho^2 + [TA - \beta_0(\bar{\rho})\bar{\rho}]P^2 + 2\frac{\alpha}{d}[TA - \beta_0(\bar{\rho})\bar{\rho}]P^3 + [TB + \frac{\alpha^2}{d^2}(TA - \beta_0(\bar{\rho})\bar{\rho})]P^4 + 4TB\frac{\alpha}{d}P^5 + [T(B' + 6B\frac{\alpha^2}{d^2})]P^6 + \beta_1(\bar{\rho})\bar{\rho}P^2\Delta\rho + 2\beta_1(\bar{\rho})\bar{\rho}\frac{\alpha}{d}P^3\Delta\rho + \beta_1(\bar{\rho})\bar{\rho}\frac{\alpha^2}{d^2}P^4\Delta\rho + o(P^6). \quad [5]$$

Analyzing Eq. 5, we infer that introducing molecular polarizability changes quantitatively the coefficients of the DFT-derived free energy but does not qualitatively affect its overall form. Specifically, when the coefficient of the P^2 term becomes zero, the same occurs for the coefficient of the P^3 term, indicating that molecular polarizability does not affect the emergence of ferroelectricity. The emergence of a tricritical point is determined by the simultaneous cancellation of the coefficients of the 2^{nd} and 4^{th} powers of P. Although introducing molecular polarizability adds a term proportional to P^3 and a negative contribution to the coefficient of the P^4 term, when the coefficient of the P^2 term, $[TA - \beta_0(\bar{\rho})\bar{\rho}]$, becomes zero, the coefficient of the P^3 term also vanishes, while the P^4 term remains $TB > 0$. This indicates that molecular polarizability alone cannot produce a tricritical phase diagram; the presence of the $\rho - P$ coupling term is essential.

V. Algebraic steps to obtain P_{eq} in mean-field DFT. In the following, the algebraic steps to obtain the P_{eq} values reported in Tabs. 1 and 2 of the main text are illustrated. Substituting ΔV_{eq} in Eq. 6 of the main text into Eq. 4 yields

$$a(T - T_c^*(p))\mathbf{P}_{eq} + B^*\mathbf{P}_{eq}^3 + B'\mathbf{P}_{eq}^5 - \mathbf{E} = 0, \quad [6]$$

with

$$T_c^*(p) = T_c - 2\frac{\beta}{aM}p^2; \quad [7]$$

$$B^* = B - \frac{2\beta^2}{M}p^2; \quad [8]$$

and

$$\bar{p}_c : B^*(\bar{p}_c) = 0; \quad [9]$$

$$\bar{T}_c = T_c^*(\bar{p}_c). \quad [10]$$

Furthermore, after setting $\mathbf{E} = 0$, χ and K_T are found to be, see Eqs. 38-39 in the main text,

$$\chi = \frac{1}{a(T - T_c^*) + 3B^*\mathbf{P}_{eq}^2 + 5B'\mathbf{P}_{eq}^4}; \quad [11]$$

$$K_T = \bar{K}_T + \Delta K_T = -\frac{1}{V}\frac{\partial \bar{V}}{\partial p} + \frac{1}{VM}\frac{a(T - T_c^*) + 3B^*\mathbf{P}_{eq}^2 + 5B'\mathbf{P}_{eq}^4 + 4\frac{(\beta p)^2}{M}\mathbf{P}_{eq}^2}{a(T - T_c^*) + 3B^*\mathbf{P}_{eq}^2 + 5B'\mathbf{P}_{eq}^4}. \quad [12]$$

It is $\bar{K}_T > 0$. In an equilibrium stable state $\chi > 0$, $K_T > 0$.

We analyze first the case $p < \bar{p}_c$, corresponding to $B^* > 0$. The algebraic solutions of Eq. 6 with $\mathbf{E} = 0$ are

$$P_{eq}^2 = 0; \quad [13]$$

$$P_{eq}^2 = -\frac{1}{2B'}B^* \pm \frac{1}{2B'}\sqrt{B^{*2} - 4a(T - T_c^*)B'} \quad [14]$$

If $B^* > 0$, the solution with the negative sign in Eq. 14 is discarded because $P_{eq}^2 \geq 0$. Simple algebraic passages furthermore show that, if $T > T_c^*$, $\chi > 0$ and $K_T > 0$ only for $P_{eq}^2 = 0$. If $T < T_c^*$, $\chi > 0$ and $K_T > 0$ only for Eq. 14 with positive sign, where $P_{eq}^2 \neq 0$. To obtain this result, it is noteworthy that the denominator of Eqs. 11 and 12, when P_{eq}^2 is given in Eq. 14 with a positive sign, is given by: $\frac{B^{*2}}{B'}[1 - \frac{4a(T-T_c^*)B'}{B^{*2}}] - \frac{B^{*2}}{B'}\sqrt{1 - \frac{4a(T-T_c^*)B'}{B^{*2}}}$. The equilibrium values of P for $p < \bar{p}_c$ so obtained are listed in Tab. 2 of the main text.

If $p > \bar{p}_c$ ($B^* < 0$), for $T < T_c^*$ in Eq. 14, we can discard the solution with the negative sign since $P_{eq}^2 \geq 0$. Simple algebraic passages show that for $B^* < 0$ the denominator of Eqs. 11 and 12 is $\frac{B^{*2}}{B'}[1 - \frac{4a(T-T_c^*)B'}{B^{*2}}] \pm \frac{B^{*2}}{B'}\sqrt{1 - \frac{4a(T-T_c^*)B'}{B^{*2}}}$. The minus sign corresponds to the minus sign in Eq. 14. For $T < T_c^*$, the solution with the positive sign in Eq. 14 leads to $\chi > 0$ and $K_T > 0$, making it stable. A more refined analysis is, however, required for $T > T_c^*$. Since P_{eq}^2 must be real, the solution in Eq. 14 can be retained only for

$$T < \bar{T} = \frac{1}{4}\frac{B^{*2}}{aB'} + T_c^*. \quad [15]$$

We notice that $\bar{T} > T_c^*$. For $T > \bar{T}$ only the solution $P_{eq}^2 = 0$ is permitted. It is, furthermore, stable because $\bar{T} > T_c^*$. The solution $P_{eq}^2 = 0$ is stable also in the temperature range $T_c^* < T < \bar{T}$. For $T_c^* < T < \bar{T}$, both solutions with positive and negative signs in Eq. 14 yield real positive values of P_{eq}^2. Considering the expression of the denominator of Eqs. 11 and 12 reported above, only the solution with the positive sign is, however, stable. In the temperature range $T_c^* < T < \bar{T}$, there are thus two stable solutions: $P_{eq}^2 = 0$ and $P_{eq}^2 = -\frac{1}{2B'}B^* + \frac{1}{2B'}\sqrt{B^{*2} - 4a(T - T_c^*)B'}$. For T:

$$T_c^* < T < \hat{T}_c = \frac{3}{16}\frac{B^{*2}}{aB'} + T_c^* < \bar{T}. \tag{16}$$

the solution $P_{eq}^2 = 0$ is metastable. Vice versa for

$$\hat{T}_c < T < \bar{T} \tag{17}$$

the solution $P_{eq}^2 \neq 0$ is metastable. This result is proven by the fact that the difference between the value of G in Eq. 3 of the main text for $P_{eq}^2 = -\frac{1}{2B'}B^* + \frac{1}{2B'}\sqrt{B^{*2} - 4a(T - T_c^*)B'} \neq 0$ and $P_{eq}^2 = 0$ is

$$\Delta G = G(P_{eq}^2 \neq 0) - G(P_{eq}^2 = 0) \propto \frac{1}{3}a(T - T_c^*) - \frac{1}{12}\frac{B^{*2}}{B'}\sqrt{1 - \frac{4a}{B^{*2}}(T - T_c^*)B'}.$$

If $T - T_c^* > \frac{3}{16}\frac{B^{*2}}{aB'}$, then $\Delta G > 0$, indicating that the solution with $P_{eq}^2 \neq 0$ is metastable. Conversely, if $T - T_c^* < \frac{3}{16}\frac{B^{*2}}{aB'}$, then $\Delta G < 0$, implying that the solution $P_{eq}^2 = 0$ is metastable. The values of P_{eq}^2 for $p > \bar{p}_c$ thus obtained are listed in Tab. 1 of the main text.

VI. Characterization of polarization collective modes in the ferroelectric phase. Hereafter, we examine the collective modes arising from the spontaneous breaking of $O(3)$ continuous symmetry, which is generated by the appearance of a non-zero P in the ferroelectric phase. This discussion provides a physical background for the results presented in *Results*, Sec. C of the main text. In the initial stage, we will focus on the emergence of Goldstone modes in the space-time correlation function of the fluctuations of the symmetry-restoring variable, namely the $\hat{p}$-transverse polarization fluctuations, $\delta P_{T\hat{p}}$. $\hat{p}$ is parallel to $\mathbf{P}_{eq}$. The memory function formalism will be employed, drawing parallels with the approach used in Ref. (5) for describing Goldstone modes in ferromagnets. However, a classical treatment will be used here. In the further stage, we characterize Goldstone modes when a coupling exists between $\hat{p}$-transverse and longitudinal fluctuations, stemming from the constant-modulus principle (6). In the final stage, we will examine fluctuations in the longitudinal polarization component, which arise from magnitude polarization fluctuations described by the empirical Landau-Khalatnikov-Tani equation (7, 8). Differently from ferromagnets, in ferroelectrics magnitude fluctuations of the order parameter can give rise to a collective mode exhibiting a propagating nature at moderately small wavevectors. The use of the constant-modulus principle, finally, enables us to establish how the magnitude polarization fluctuations impact the correlation function of $\hat{p}$-transverse polarization.

Let a reference system be defined by the unit vectors $\hat{p}$, $\hat{t}$, and $\hat{s}$. The directions $\hat{t}$ and $\hat{s}$ are thus $\hat{p}$-transverse. The invariance of the system's Hamiltonian H under the $\hat{s}$-component of the Hermitian angular momentum operator $L_{\hat{s}}$ implies

$$\{H, L_{\hat{s}}\} = 0, \tag{18}$$

where $\{\}$ stands for Poisson bracket. As a general expression, it is

$$< \{L_{\hat{s}}, P_{\hat{t}}(\mathbf{r})\} >= -\int d\mathbf{p}d\mathbf{q}\ P_{\hat{t}}(\mathbf{q},\mathbf{p})\{L_{\hat{s}}, \rho(\mathbf{q},\mathbf{p})\} = \epsilon_{\hat{s}\hat{t}\hat{p}} < P_{\hat{p}}(\mathbf{r}) >, \tag{19}$$

where $\rho(\mathbf{q},\mathbf{p})$ is the probability density, $(\mathbf{q},\mathbf{p})$ are the canonical variables, $\epsilon_{\hat{s}\hat{t}\hat{p}}$ is the Levi-Civita symbol, $\mathbf{r}$ is the space variable, and $< >$ states for ensemble average. If $< P_{\hat{p}}(\mathbf{r}) > \neq 0$, as in the ferroelectric phase where $< P_{\hat{p}}(\mathbf{r}) >= P_{eq} \neq 0$, Eq. 19 implies that the thermodynamic state described by $\rho(\mathbf{q},\mathbf{p})$ breaks the continuous rotational symmetry $O(3)$ associated with $L_{\hat{s}}$. Because $< P_{\hat{t}} >= 0$, $\delta P_{\hat{t}} = P_{\hat{t}}$. Following a general statement, the response function, $\chi''_{L_{\hat{s}},P_{\hat{t}}}(\mathbf{r},t)$, is given by

$$\chi''_{L_{\hat{s}},P_{\hat{t}}}(\mathbf{r},t) = \frac{i}{2} < \{l_{\hat{s}}(\mathbf{r},t), P_{\hat{t}}(\mathbf{0},0)\} >, \tag{20}$$

where t is the time variable. $l_{\hat{s}}(\mathbf{r},t)$ is the local and time-dependent angular momentum operator. It is $L_{\hat{s}}(t) = \int d\mathbf{r}\ l_{\hat{s}}(\mathbf{r},t)$. In the space- and time-Fourier conjugate variables, the wavevector $\mathbf{k}$ and frequency ω respectively, the response function is

$$\chi''_{L_{\hat{s}},P_{\hat{t}}}(\mathbf{k},\omega) = \int_{-\infty}^{\infty} dt \int_{-\infty}^{\infty} d\mathbf{r}\ e^{i\omega t - i\mathbf{k}\cdot\mathbf{r}}\chi''_{L_{\hat{s}},P_{\hat{t}}}(\mathbf{r},t), \tag{21}$$

Form Eq. 19, considering that $< P_{\hat{p}}(\mathbf{r}) >= P_{eq}$, it is found

$$\chi''_{\hat{L}_{\hat{s}},P_{\hat{t}}}(\mathbf{k}=0,\omega) = \frac{i}{2}\ P_{eq}\ \delta(\omega). \tag{22}$$

If the function $\chi''_{\hat{L}_{\hat{s}},P_{\hat{t}}}(\mathbf{k},\omega)$ is well-behaved in the small-k region, which is ensured by the fast decay of the response function in $\mathbf{r}$ (5), then one can extend the applicability of Eq. 22 to the limit $k \to 0$. This establishes

$$\lim_{k\to 0}\chi''_{\hat{L}_{\hat{s}},P_{\hat{t}}}(\mathbf{k},\omega) = \frac{i}{2}\ P_{eq}\ \delta(\omega). \tag{23}$$

By leveraging the Bogoliubov inequality (5), and employing Eq. 19 under the condition of continuous symmetry breaking $< P_{\hat{p}}(\mathbf{r}) >= P_{eq} \neq 0$, it is possible to demonstrate the divergence of the static susceptibility of $P_{\hat{t}}$, $\chi_{P_{\hat{t}}P_{\hat{t}}}$, in the macroscopic limit $k \to 0$ using the same methodology outlined in Ref. (5) for ferromagnets. Specifically, it is

$$\lim_{k\to 0} \chi_{P_{\hat{t}}P_{\hat{t}}}(k) = \frac{P_{eq}^2}{c_P k^2}, \tag{24}$$

where $c_P = \lim_{k\to 0} \int \frac{d\omega}{\pi\omega} \chi''_{J_{L_{\hat{s}}} J_{L_{\hat{s}}}}(k,\omega)$. $J_{L_{\hat{s}}}$ is the current density of $L_{\hat{s}}$. The divergence of the transverse to $\hat{p}$ static susceptibility as $k \to 0$ in the ferroelectric phase, scaling as k^{-2}, is thus a direct consequence of the breaking of the continuous $O(3)$ symmetry due to the emergence of spontaneous polarization. In the following, by exploiting the memory function formalism, we will show how the emergence of so-called Goldstone modes is linked to Eq. 24, thus resulting ultimately related to the breaking of the continuous $O(3)$ symmetry, in accordance with the Goldstone theorem.

For the sake of clarity, we introduce below the quantities involved in the memory function formalism and summarize its principal findings (5, 9, 10). We assume the Boltzmann constant $K_B = 1$. Under time and space translational invariance the space-time correlation function between variables A_i and A_j, with $< A_i >=< A_j >= 0$ is

$$C_{ij}(\mathbf{r},t) =< A_i(\mathbf{r},t) A_j(\mathbf{0},0) > . \tag{25}$$

The space- and time-Fourier transform of Eq. 25 is

$$C_{ij}(\mathbf{k},\omega) = \int_{-\infty}^{\infty} dt \int_{-\infty}^{\infty} d\mathbf{r}\; e^{i\omega t - i\mathbf{k}\cdot\mathbf{r}} C_{ij}(\mathbf{r},t). \tag{26}$$

Its time-Laplace transform and space-Fourier transform is

$$\tilde{C}_{ij}(\mathbf{k},z) = \int_{0}^{\infty} dt\; e^{izt} C_{ij}(\mathbf{k},t); \qquad z \in \mathbb{C}^+. \tag{27}$$

z is the Laplace-conjugate variable of t. The following relationships can be proved (5):

$$\tilde{C}_{ij}(\mathbf{k},z) = \int_{-\infty}^{\infty} \frac{d\omega}{2\pi i} \frac{C_{ij}(\mathbf{k},\omega)}{\omega - z}; \tag{28}$$

$$C_{ij}(\mathbf{k},\omega) = \lim_{\epsilon\to 0} 2\mathrm{Re}(\tilde{C}_{ij}(\mathbf{k},\omega + i\epsilon)), \tag{29}$$

where $\mathrm{Re}(x)$ is the real part of the complex number x. The fluctuation-dissipation theorem establishes that

$$C_{ij}(\mathbf{k},\omega) = T \frac{2\chi''_{ij}(\mathbf{k},\omega)}{\omega}. \tag{30}$$

The correlation function can be written as

$$C_{ij}(\mathbf{k},t) =< A_i(\mathbf{k},0) e^{-i\mathcal{L}t} A_j(\mathbf{k},0) >, \tag{31}$$

and in the Laplace-space

$$\tilde{C}_{ij}(\mathbf{k},z) =< A_i(\mathbf{0},0) \frac{i}{z - \mathcal{L}} A_j(\mathbf{0},0) >, \tag{32}$$

where $\mathcal{L}$ is the Liouville operator. The core of the memory function formalism (5, 9, 10) is the introduction of a Hilbert space of observables $|A_i>$ where the scalar product between the two elements $|A_i>$ and $|A_j>$ is defined as

$$< A_i | A_j >=< A_i A_j > . \tag{33}$$

The projection operator, $\mathcal{P}$ and its complement $\mathcal{Q}$ are defined by

$$\mathcal{P} = \sum_{ij} |A_i(0)>< A_i(0)|A_j(0)>< A_j(0)| = I - \mathcal{Q}, \tag{34}$$

where I is the identity operator. The correlation function $\tilde{C}_{ij}(\mathbf{k},z)$ is then given as

$$\tilde{C}_{ij}(\mathbf{k},z) = T \frac{i\chi_{ij}(\mathbf{k})}{z\delta_{ij} - \Omega_{ij}(\mathbf{k}) - i\Sigma_{ij}(\mathbf{k},z)}. \tag{35}$$

It is

$$\chi_{ij}(\mathbf{k}) = T^{-1} < A_i(\mathbf{k},0) | A_j(\mathbf{k},0) >= \int_{-\infty}^{\infty} \frac{d\omega}{\pi} \frac{\chi''_{ij}(\mathbf{k},\omega)}{\omega}; \tag{36}$$

$$\Omega_{ij}(\mathbf{k}) = \omega_{ik} \chi^{-1}_{kj},$$

$$\omega_{ij} = T^{-1} i < \dot{A}_i(\mathbf{k},0) | A_j(\mathbf{k},0) >= \int_{-\infty}^{\infty} \frac{d\omega}{\pi} \chi''_{ij}(\mathbf{k},\omega), \tag{37}$$

where $\dot{A}_i(t) = \frac{d}{dt}A_i(t)$ is the time derivative of $A_i(t)$. The memory matrix $\Sigma_{ij}(\mathbf{k}, z)$ is

$$\Sigma_{ij}(\mathbf{k}, z) = \sigma_{ik}(\mathbf{k}, z)\chi^{-1}_{kj}, \tag{38}$$

$$\sigma_{ij}(\mathbf{k}, z) = T^{-1} < \dot{A}_i(\mathbf{k}, 0)|\mathcal{Q}\frac{i}{z - \mathcal{QLQ}}\mathcal{Q}|\dot{A}_j(\mathbf{k}, 0) > . \tag{39}$$

If $\Omega_{ij} \neq 0$, C_{ij} is characterized by a propagating mode. $\chi_{ij}(\mathbf{k})$ is the static susceptibility.

The correlation function $C_{P_{\hat{t}}P_{\hat{t}}}$ in the ferroelectric phase is derived in the following by exploiting the memory function formalism. Because of Eq. 19 the variables $L_{\hat{s}}$ and $P_{\hat{t}}$ are correlated. Consequently, we will consider the set of variables $|L_{\hat{s}} >, |P_{\hat{t}} >$. It's beneficial to note that $\mathbf{L} = (L_{\hat{p}}, L_{\hat{t}}, L_{\hat{s}})$ is odd under parity and odd under time reversal, whereas $\mathbf{P} = (P_{\hat{p}}, P_{\hat{t}}, P_{\hat{s}})$ is odd under parity and even under time reversal. Moreover, according to Eq. 19, $\chi''_{L_{\hat{s}}P_{\hat{t}}} = -\chi''_{L_{\hat{t}}P_{\hat{s}}}$. To the lowest order in k we find

$$\chi_{L_{\hat{s}}P_{\hat{t}}}(\mathbf{k}) = \begin{pmatrix} \frac{P_{eq}^2}{c_L k^2} & 0 \\ 0 & \frac{P_{eq}^2}{c_P k^2} \end{pmatrix}, \tag{40}$$

where $c_L = \lim_{k\to 0} \frac{1}{k^2} \int \frac{d\omega}{\pi\omega}\chi''_{J_{P_{\hat{t}}}J_{P_{\hat{t}}}}(k, \omega)$. $J_{P_{\hat{t}}}$ is the current density of $P_{\hat{t}}$. The off-diagonal elements are equal to zero due to time reversal symmetry. The diagonal element $\chi_{P_{\hat{t}}P_{\hat{t}}}$ is obtained from Eq. 24. Similarly, the diagonal element $\chi_{L_{\hat{s}}L_{\hat{s}}}$ is obtained from the Bogoliubov inequality and considering that $P_{\hat{t}}$ is conserved. If this were not the case, the diagonal element in the first row of the susceptibility matrix, Eq. 40, would be constant in k. The ω_{ij} matrix is

$$\omega_{L_{\hat{s}}P_{\hat{t}}}(\mathbf{k}) = \begin{pmatrix} 0 & i\ P_{eq} \\ -i\ P_{eq} & 0 \end{pmatrix}. \tag{41}$$

The diagonal elements are equal to zero due to time reversal invariance, whereas the off-diagonal elements can be easily computed from Eq. 37 and Eqs. 19-20. From Eq. 39 and the continuity equation holding for conserved variables, to leading order in k (5) it is found

$$\sigma_{L_{\hat{s}}P_{\hat{t}}}(\mathbf{k}) = \begin{pmatrix} \gamma_{LL}k^2 & \gamma_{LP}k^2 \\ -\gamma_{LP}k^2 & \gamma_{PP}k^2 \end{pmatrix}. \tag{42}$$

All the elements of the memory matrix should be real, but only the diagonal elements are constrained to be positive since they are identified with dissipative terms. In writing Eq. 42 it is implicitly assumed that i) $\exists \lim_{z\to 0} \sigma_{ij}(k, z) < \infty$; ii) $\exists \lim_{k\to 0} \sigma_{ij}(k, 0) < \infty$, where in this case $i, j = L_{\hat{s}}, P_{\hat{t}}$. A heuristic proof of these claims for generic i, j is given in Ref. (5). We then exploit Eq. 35 and, to the leading order in k, we obtain for the limit $k \to 0$,

$$\tilde{C}_{P_{\hat{t}},P_{\hat{t}}}(\mathbf{k}, z) = T\frac{iP_{eq}^2}{c_P k^2}\frac{z + i\gamma_{PP}\frac{c_P}{P_{eq}^2}k^4}{z^2 - \frac{c_P c_L}{P_{eq}^2}k^4 + 2iz\gamma_{PP}\frac{c_P}{P_{eq}^2}k^4}; \tag{43}$$

By making use of Eq. 29, it is then easily derived $C_{P_{\hat{t}},P_{\hat{t}}}(\mathbf{k}, \omega)$. It is characterized by a propagating mode with associated dispersion equation

$$\omega(k) = \frac{\sqrt{c_P c_L}}{P_{eq}}k^2. \tag{44}$$

The phase velocity of the propagating mode decreases by decreasing the wavevector. This behavior arises from the conservation of the symmetry-restoring variable. Without it, Eq. 40 would feature only one diagonal element proportional to k^{-2}, changing the dispersion of Goldstone modes in Eq. 44 into $\omega(k) \propto k$ as in usual sound waves. The damping $\Gamma(k)$ of the propagating mode is obtained from Eq. 43, $\Gamma(k) = 2\gamma_{PP}\frac{c_P}{P^2}k^4$. In the hydrodynamic limit $k \to 0$ the Goldstone mode will thus be not overdamped because the condition $\Gamma^2(k) < \omega(k)^2$ will be met. However, at moderately small values of k, the mode may become overdamped depending on the specific values of the parameters in Eq. 44.

The constant modulus principle (6) establish that

$$\delta P_{\hat{p}} = -\frac{\delta P_{\hat{t}}^2}{P_{eq}}. \tag{45}$$

A correlation is thus introduced between $\hat{p}$-transverse and longitudinal polarization fluctuations. As a consequence (6), a divergence in the macroscopic limit exists also in the $\hat{p}$-longitudinal polarization static susceptibility,

$$\chi_{P_{\hat{p}}P_{\hat{p}}}(\mathbf{k}) = \frac{P_{eq}^2}{c_P k}. \tag{46}$$

In the upcoming analysis, our aim is to investigate the impact of the constant modulus principle on the dynamics of both transverse and longitudinal polarization fluctuations. To achieve this, the set of dynamical variables subject to the memory function formalism needs to be expanded to $|L_s >, |P_{\hat{t}} >, |\delta P_{\hat{p}} >$, given the existing correlation between $\hat{p}$-transverse and longitudinal polarization fluctuations established by Eq. 45. The static susceptibility matrix to lowest order in k is obtained from Eq. 40 and Eq. 46,

$$\chi_{L_{\hat{s}}P_{\hat{t}}P_{\hat{p}}}(\mathbf{k}) = \begin{pmatrix} \frac{P_{eq}^2}{c_L k^2} & 0 & 0 \\ 0 & \frac{P_{eq}^2}{c_P k^2} & 0 \\ 0 & 0 & \frac{P_{eq}^2}{c_p k} \end{pmatrix}. \tag{47}$$

The response function $\chi''_{L_{\hat{s}},P_{\hat{p}}}$ to the lowest order in k is equal to zero. It is indeed

$$\chi''_{L_{\hat{s}},P_{\hat{p}}} =< \{L_{\hat{s}}, \delta P_{\hat{p}}(\mathbf{r})\} >=< P_{\hat{t}}(\mathbf{r}) >= 0. \tag{48}$$

Moreover, $\chi''_{P_{\hat{t}},P_{\hat{p}}} = 0$ because

$$\chi''_{P_{\hat{t}},P_{\hat{p}}} =< \{L_{\hat{s}} \times \delta P_{\hat{p}}(\mathbf{r}), \delta P_{\hat{p}}(\mathbf{r})\} >= \; < \{L_{\hat{s}}, \delta P_{\hat{p}}(\mathbf{r})\} \times \delta P_{\hat{p}}(\mathbf{r}) >=< P_{\hat{s}}(\mathbf{r}) >= 0. \tag{49}$$

Finally, it is

$$\chi''_{L_{\hat{s}},P_{\hat{t}}} =< \{L_{\hat{s}}, P_{\hat{t}}(\mathbf{r})\} >=< P_{\hat{p}}(\mathbf{r}) >= P_{eq}. \tag{50}$$

The frequency matrix is thus

$$\omega_{L_{\hat{s}}P_{\hat{t}}P_{\hat{p}}}(\mathbf{k}) = \begin{pmatrix} 0 & iP_{eq} & 0 \\ -iP_{eq} & 0 & 0 \\ 0 & 0 & 0 \end{pmatrix}. \tag{51}$$

The diagonal elements are equal to zero because of time-reversal invariance. The memory matrix is

$$\sigma_{\hat{L}_{\hat{s}}P_{\hat{t}}}(\mathbf{k}) = \begin{pmatrix} \gamma_{LL}k^2 & \gamma_{LPt}k^2 & \gamma_{LPp}k^2 \\ -\gamma_{LPt}k^2 & \gamma_{PtPt}k^2 & \gamma_{PtPp}k^2 \\ -\gamma_{LPp}k^2 & -\gamma_{PtPp}k^2 & \gamma_{PpPp}k^2 \end{pmatrix}. \tag{52}$$

After algebraic passages and taking into account only the leading terms in k it is obtained,

$$\tilde{C}_{P_{\hat{t}}P_{\hat{t}}}(\mathbf{k}, z) = iT \frac{P_{eq}^2}{c_P k^2} \frac{z + 2i\gamma_{P_{\hat{t}}P_{\hat{t}}} c_P k^4}{z^2 - \frac{c_P c_L k^4}{P^2} + iz\gamma_{P_{\hat{t}}P_{\hat{t}}} c_P k^4} + O(k^3); \tag{53}$$

$$\tilde{C}_{P_{\hat{p}}P_{\hat{p}}}(\mathbf{k}, z) = iT \frac{P_{eq}^2}{c_P k} \frac{1}{z + i\gamma_{P_{\hat{p}}P_{\hat{p}}} c_P k^3} + O(k^2). \tag{54}$$

Eqs. 53 and 54 show that under the validity of Eq. 45, the correlation function of transverse fluctuations in the small k's limit is yet characterized by a propagating mode, whereas the longitudinal correlation function exhibits a diffusive mode with the unusual k-dependent diffusion coefficient, $D_{\hat{t}}^2(k) = \gamma_{P_{\hat{p}}P_{\hat{p}}} R_P k^3$.

The results obtained so far are derived under the hypothesis that fluctuations of the Gibbs free energy are driven by $\hat{p}$-transverse polarization fluctuations. Fluctuations in the polarization magnitude, which cause $\hat{p}$-longitudinal polarization fluctuations, have been considered negligible. As specified in the main text, their dynamics is empirically described by the Landau-Khalatnikov-Tani equation (7, 8). This leads to a collective mode in the space-time correlation function of $\delta P_{\hat{p}}$, exhibiting propagating behavior with a linear dispersion relation at moderately small k values (7), and converging to a constant as $k \to 0$. Under the assumption that the constant modulus principle holds — i.e., the lowest-order fluctuations tend to preserve the polarization magnitude — spontaneous fluctuations in polarization magnitude, initially resulting in $\hat{p}$-longitudinal polarization fluctuations, will also be reflected as $\hat{p}$-transverse polarization fluctuations, as described by Eq. 45. Making the simplifying assumption that $\delta P_{\hat{p}}$ behaves as a Gaussian random field, and dismissing the damping term, it is

$$\tilde{C}_{P_{\hat{p}}P_{\hat{p}}}(\mathbf{k}, z) \propto \frac{z}{z^2 - \Omega_o^2 - gk^2}. \tag{55}$$

Exploiting Eq. 45 and yet under the assumption of Gaussian field for $\tilde{C}_{P_{\hat{p}}P_{\hat{p}}}(\mathbf{k}, z)$, we derive $\tilde{C}_{P_{\hat{t}}P_{\hat{t}}}(\mathbf{k}, z) \propto \tilde{C}^2_{P_{\hat{p}}P_{\hat{p}}}(\mathbf{k}, z)$. Using Eq. 29 and the generalization of the Sokhotski-Plemelj theorem due to Fox (11) it is possible to show (12) that $C_{P_{\hat{t}}P_{\hat{t}}}(\mathbf{k}, \omega)$, as well as $C_{P_{\hat{p}}P_{\hat{p}}}(\mathbf{k}, \omega)$, exhibit a pole at $\omega^2 = \Omega_0^2 + gk^2$. In other words, both correlation functions have a collective mode with the same dispersion relation.

VII. Polarization and density space-time correlation functions in the (p, T) plane from MD simulations. Figs. S7-S8 show, at different k values, $C_{T\hat{p}T\hat{p}}(k, t)$, $C_{L\hat{p}L\hat{p}}(k, t)$, $C_{PP}(k, t)$, $C_{\rho\rho}(k, t)$ along the line $p = 1000$ bar for different T's crossing the WL. The oscillatory behavior, associated with propagating collective modes caused by the spontaneous symmetric breaking of the ferroelectric LDL, gradually disappears upon crossing the WL. In the paraelectric HDL, these modes are completely absent, and the correlation function relaxes to zero on a timescale much shorter than μs. Figs. S9-S10 show the same quantities along the line $p = 0$ bar for different T's crossing the WL. Fig. S11 depicts $C_{T\hat{p}T\hat{p}}(k, t)$, $C_{L\hat{p}L\hat{p}}(k, t)$, $C_{PP}(k, t)$, and $C_{\rho\rho}(k, t)$ along the line $p = 2500$ bar just above and below the first-order LLPT line, where the characteristics of spontaneous symmetry breaking manifest. Fig. S12 shows these same quantities close to CP, where phase coexistence is observed. Notice that the correlation functions in Figs. S7-S12 have different time-length. Fig. S13 show $\chi_{T\hat{p}(L\hat{p})}(k)$ in LDL at different points of the thermodynamic plane (p, T).

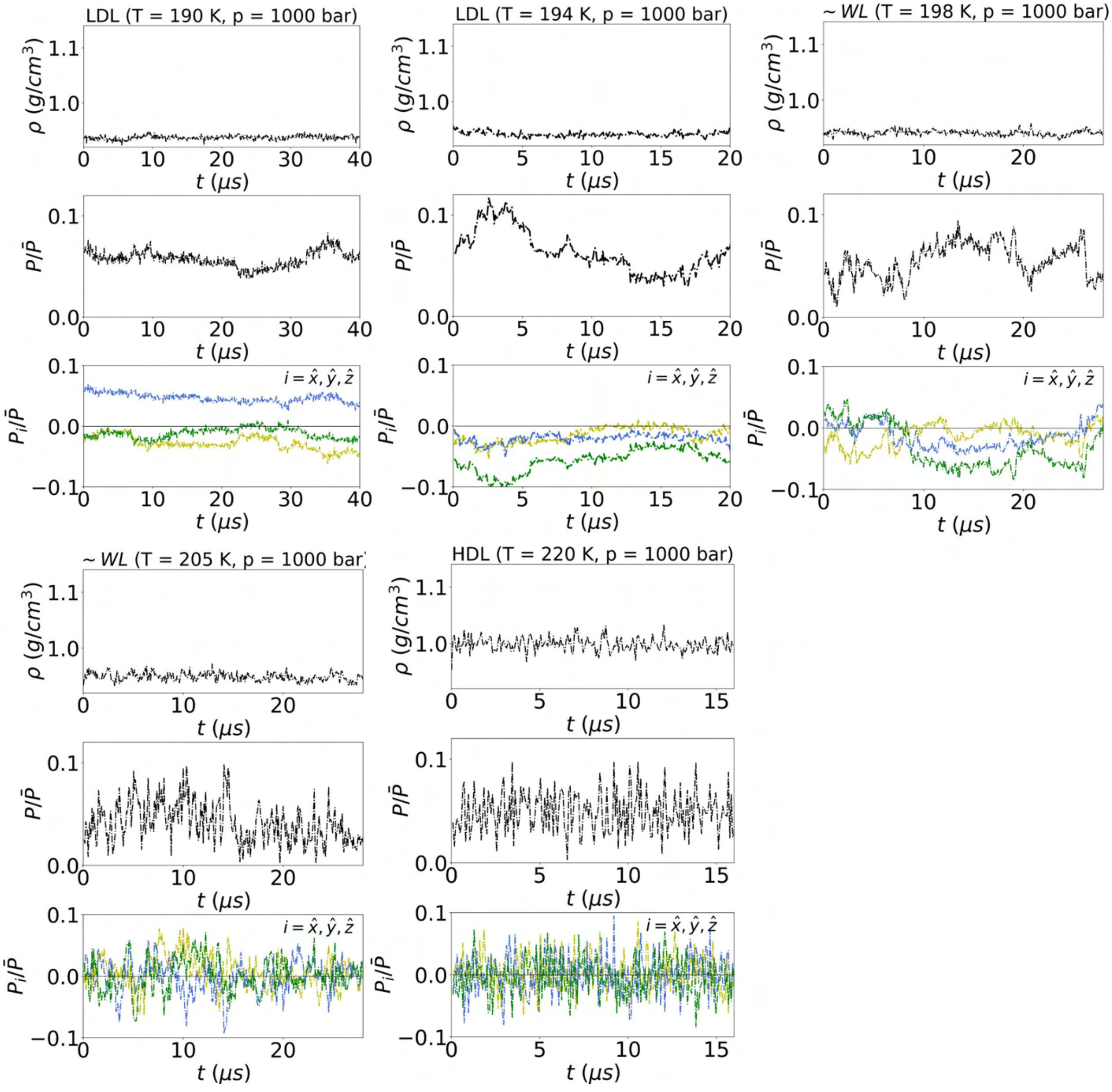

Fig. S1. Temporal evolution of ρ (top), P (middle), and P_i (bottom) at different points in the (p, T) plane along the $p = 1000$ bar line crossing the WL. It is $\bar{P} = Nd$.

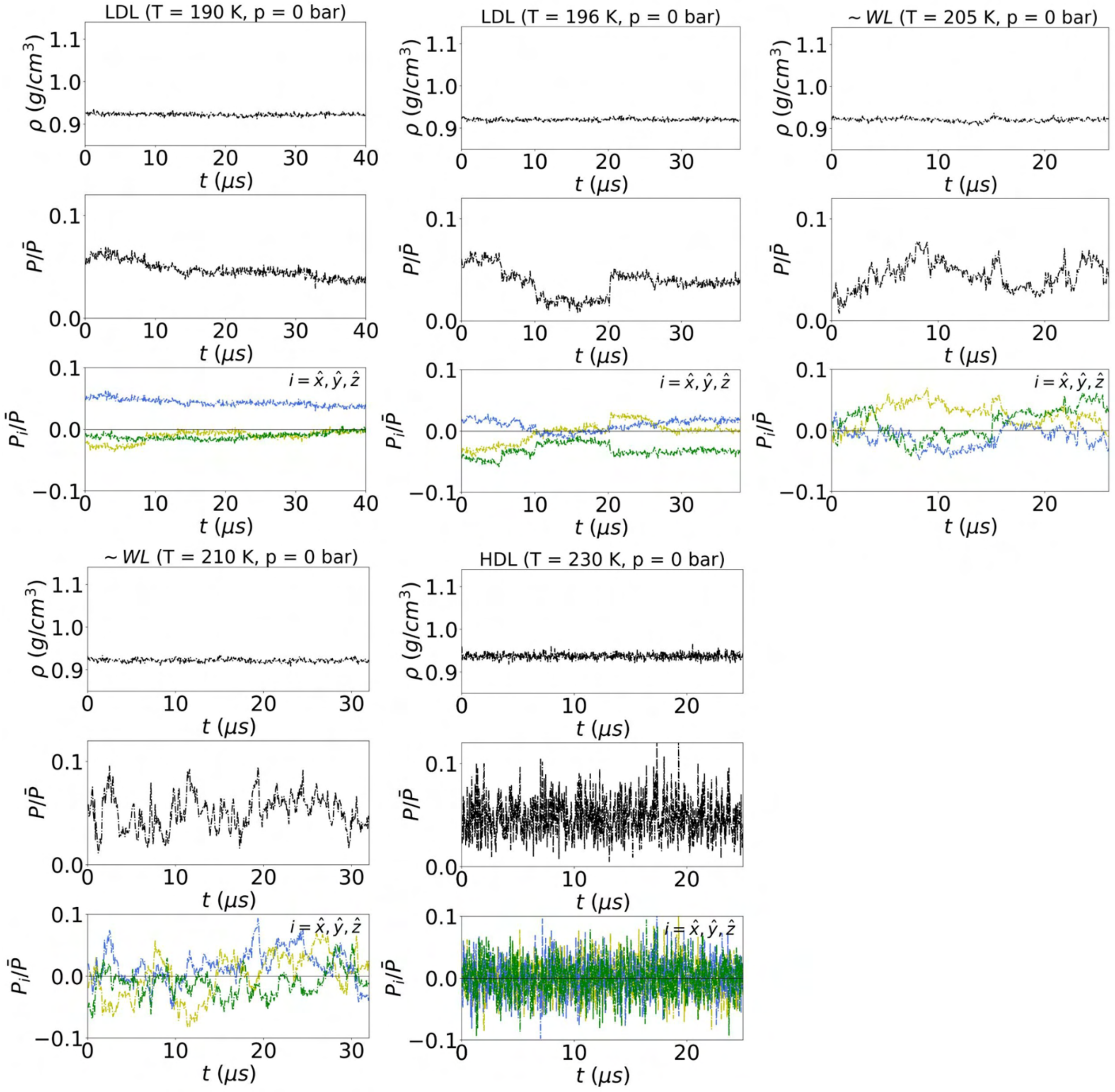

Fig. S2. Temporal evolution of ρ (top), P (middle) and P_i (bottom) in different points of the (p, T) plane along the $p = 0$ bar line crossing the WL. It is $\bar{P} = Nd$.

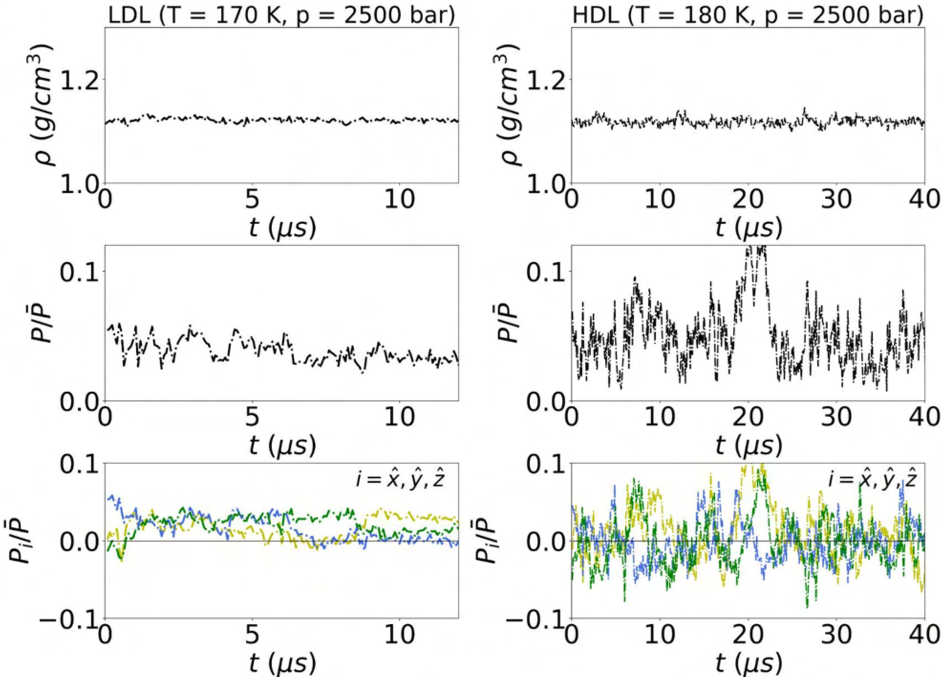

Fig. S3. Temporal evolution of ρ (top), P (middle) and P_i (bottom) in different points of the (p, T) plane along the line $p = 2500$ bar crossing the first-order LLPT line. It is $\bar{P} = Nd$.

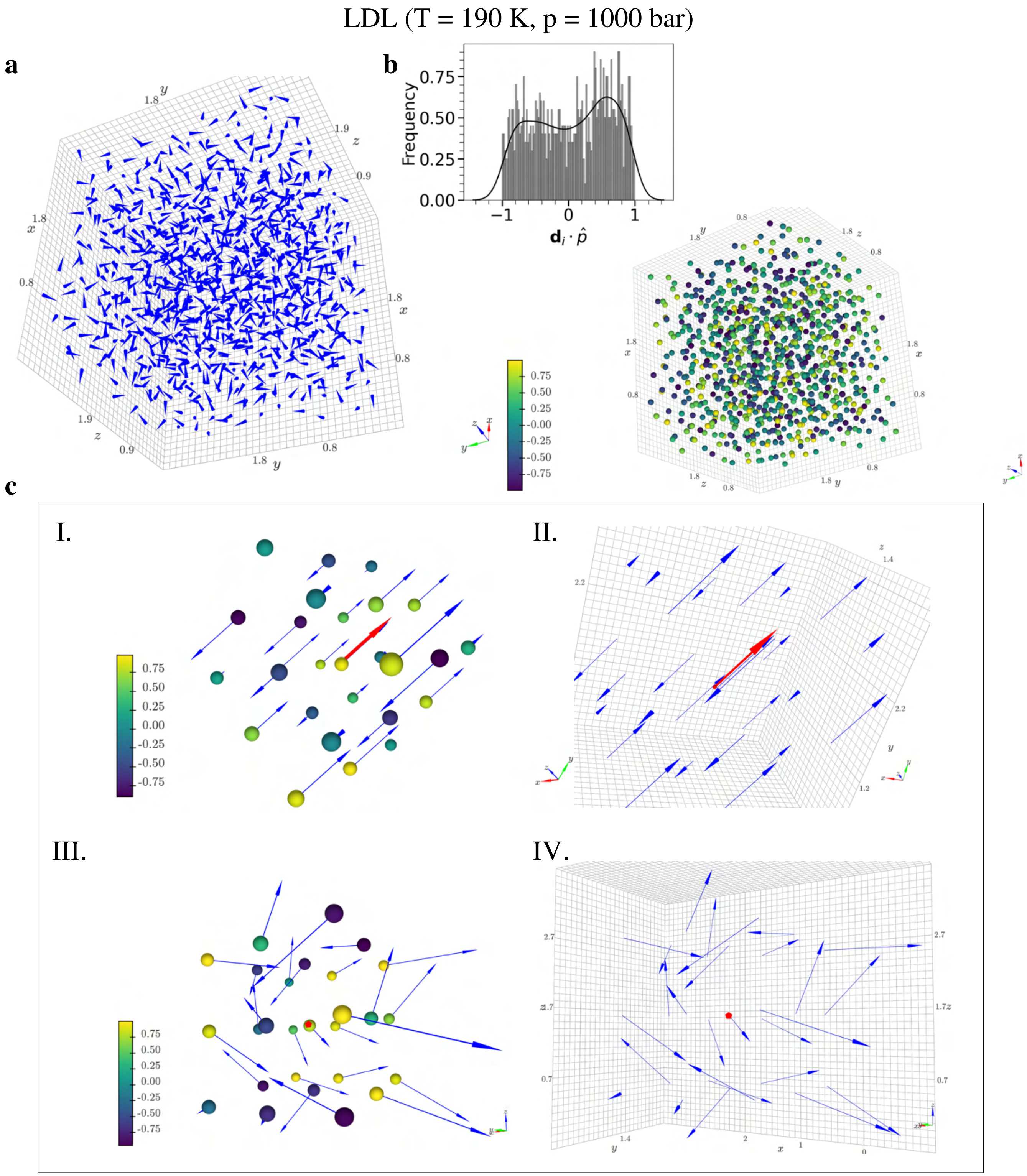

Fig. S4. *Panel a.* Spatial distribution of $\mathbf{d}_i$ in LDL: arrows represent the dipole orientation in a single MD simulation configuration. The arrowheads are positioned at the centers of mass of each molecule, with the arrows pointing in the direction of the molecular dipole. The magnitude of instantaneous polarization $\mathbf{P}(t)$ is $P(t)/Nd_i = 0.053$. *Panel b.* The bottom graph shows the spatial distribution of $\frac{\mathbf{d}_i}{d_i} \cdot \hat{p}$, where $\hat{p}$ is the unit vector along $\mathbf{P}(t)$. The scalar product is represented by the color of the circles at the center of mass of each molecule, as indicated by the color bar. The top graph displays the frequency distribution of $\mathbf{d}_i \cdot \hat{p}$. *Panel c.* Graphical representation of the spatial distribution of $\mathbf{D}_i$, the dipole vector of the i-th cell, where the simulation box is evenly divided into cells of size $L/3$, with L being the simulation box size. The red arrow indicates the direction of $\mathbf{P}(t)$. The projection of $\mathbf{D}_i/D_i$ along $\hat{p}$, $\mathbf{D}_{i\parallel\hat{p}} = \mathbf{D}_i/D_i \cdot \hat{p}\,\hat{p}$, is shown by arrows in graphs *I* and *II*. In graph *I*, the color of the circles at the center of mass of each i-th cell represents the scalar product $\frac{\mathbf{D}_i}{D_i} \cdot \hat{p}$ for better visualization. The projection of $\mathbf{D}_i/D_i$ on the plane orthogonal to $\hat{p}$, $\mathbf{D}_{i\perp\hat{p}} = \mathbf{D}_i/D_i - \mathbf{D}_i/D_i \cdot \hat{p}\,\hat{p}$ is shown by arrows in graphs *III* and *IV*. In graph *IV*, the color of the circles at the center of mass of each i-th cell represents the scalar product $\mathbf{D}_{i\perp\hat{p}} \cdot \bar{\mathbf{D}}_{\perp\hat{p}}$ for better visualization, where $\bar{\mathbf{D}}_{\perp\hat{p}}$ is the average of $\mathbf{D}_{i\perp\hat{p}}$. The observation plane is orthogonal to $\mathbf{P}(t)$, which points out of the plane of the page.

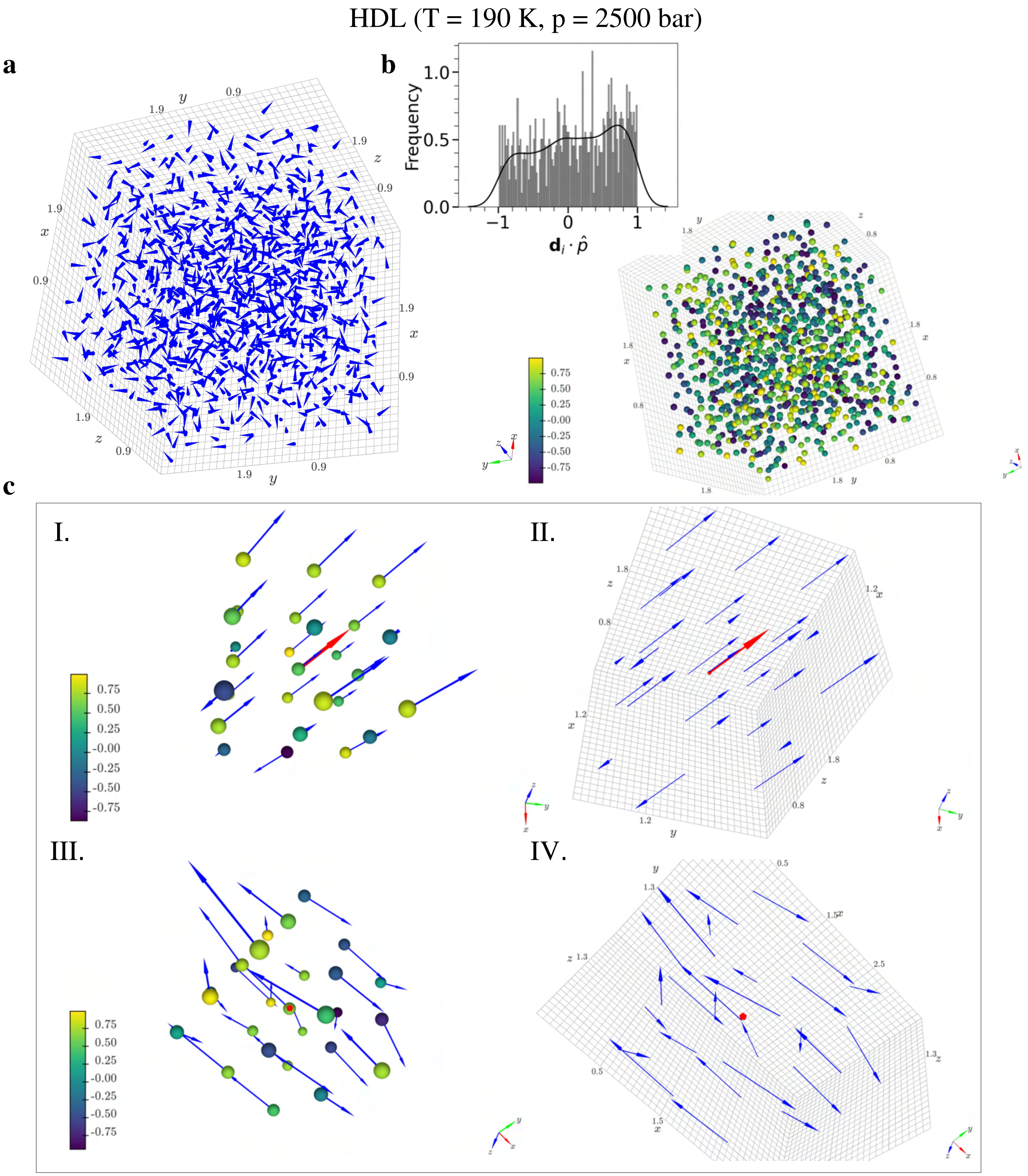

Fig. S5. *Panel a.* Spatial distribution of $\mathbf{d}_i$ in HDL: arrows represent the dipole orientation in a single MD simulation configuration. The arrowheads are positioned at the centers of mass of each molecule, with the arrows pointing in the direction of the molecular dipole. The magnitude of instantaneous polarization $\mathbf{P}(t)$ is $P(t)/Nd_i = 0.095$. *Panel b.* The bottom graph shows the spatial distribution of $\frac{\mathbf{d}_i}{d_i} \cdot \hat{p}$, where $\hat{p}$ is the unit vector along $\mathbf{P}(t)$. The scalar product is represented by the color of the circles at the center of mass of each molecule, as indicated by the color bar. The top graph displays the frequency distribution of $\mathbf{d}_i \cdot \hat{p}$. *Panel c.* Graphical representation of the spatial distribution of $\mathbf{D}_i$, the dipole vector of the i-th cell, where the simulation box is evenly divided into cells of size $L/3$, with L being the simulation box size. The red arrow indicates the direction of $\mathbf{P}(t)$. The projection of $\mathbf{D}_i/D_i$ along $\hat{p}$, $\mathbf{D}_{i\parallel\hat{p}} = \mathbf{D}_i/D_i \cdot \hat{p}\,\hat{p}$, is shown by arrows in graphs *I* and *II*. In graph *I*, the color of the circles at the center of mass of each i-th cell represents the scalar product $\frac{\mathbf{D}_i}{D_i} \cdot \hat{p}$ for better visualization. The projection of $\mathbf{D}_i/D_i$ on the plane orthogonal to $\hat{p}$, $\mathbf{D}_{i\perp\hat{p}} = \mathbf{D}_i/D_i - \mathbf{D}_i/D_i \cdot \hat{p}\,\hat{p}$ is shown by arrows in graphs *III* and *IV*. In graph *IV*, the color of the circles at the center of mass of each i-th cell represents the scalar product $\mathbf{D}_{i\perp\hat{p}} \cdot \bar{\mathbf{D}}_{\perp\hat{p}}$ for better visualization, where $\bar{\mathbf{D}}_{\perp\hat{p}}$ is the average of $\mathbf{D}_{i\perp\hat{p}}$. The observation plane is orthogonal to $\mathbf{P}(t)$, which points out of the plane of the page.

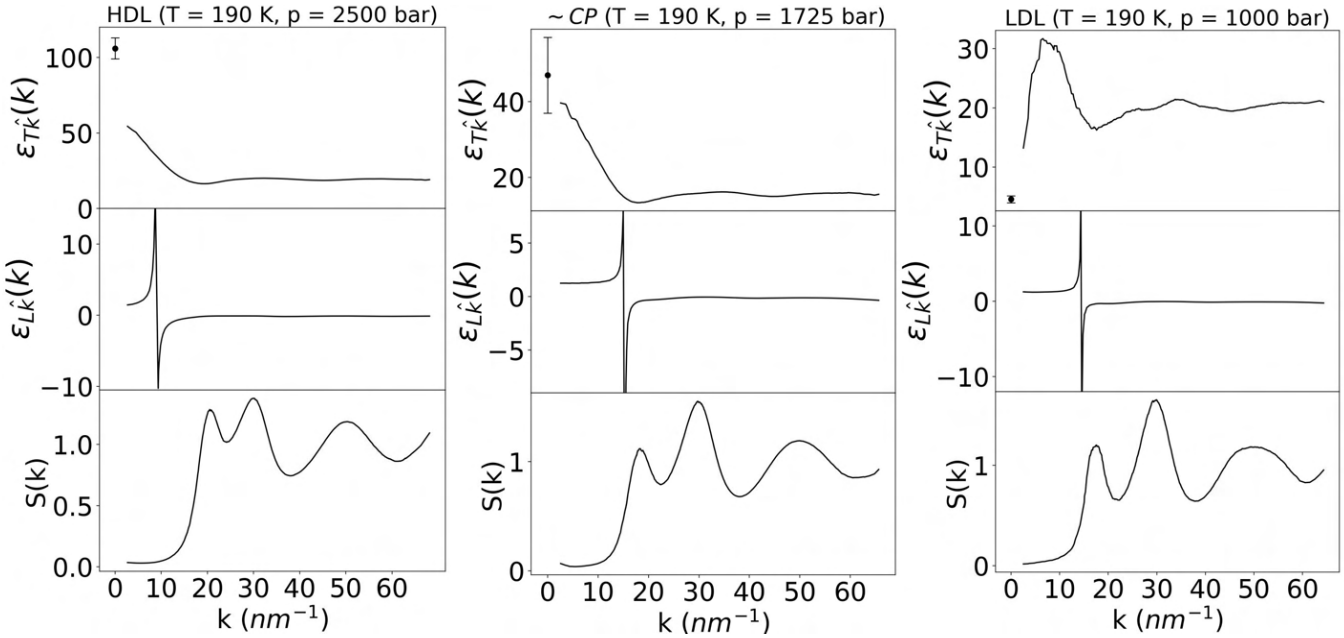

Fig. S6. Non-local transverse (longitudinal) static dielectric functions, $\epsilon_{T(L)}(k)$ and static structure factor $S(k)$ in HDL, close to CP and in LDL. The black circle with the error bar, obtained by block averaging, in the upper graphs mark the value of ϵ_0. The first peak in $S(k)$ corresponds to a minimum in $\epsilon_T(k)$, highlighting a possible link between the spatial arrangement of molecules' center of mass and dipole orientation.

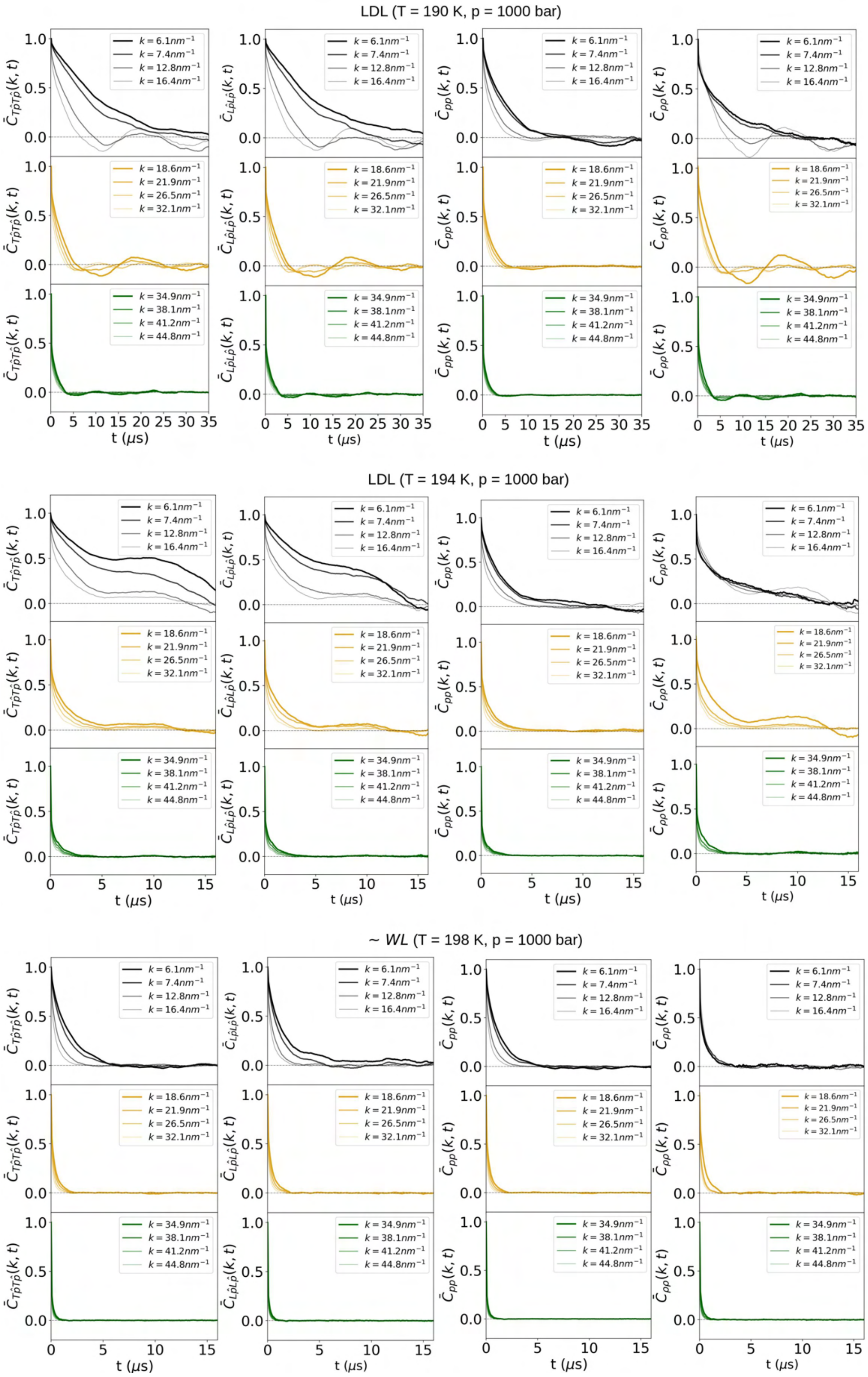
LDL (T = 190 K, p = 1000 bar)

LDL (T = 194 K, p = 1000 bar)

~ *WL* (T = 198 K, p = 1000 bar)

Fig. S7. Normalized $C_{T\hat{p}T\hat{p}}(k,t)$, $C_{L\hat{p}L\hat{p}}(k,t)$, $C_{PP}(k,t)$, $C_{\rho\rho}(k,t)$ at different T's along the $p = 1000$ bar isobar, crossing the WL.

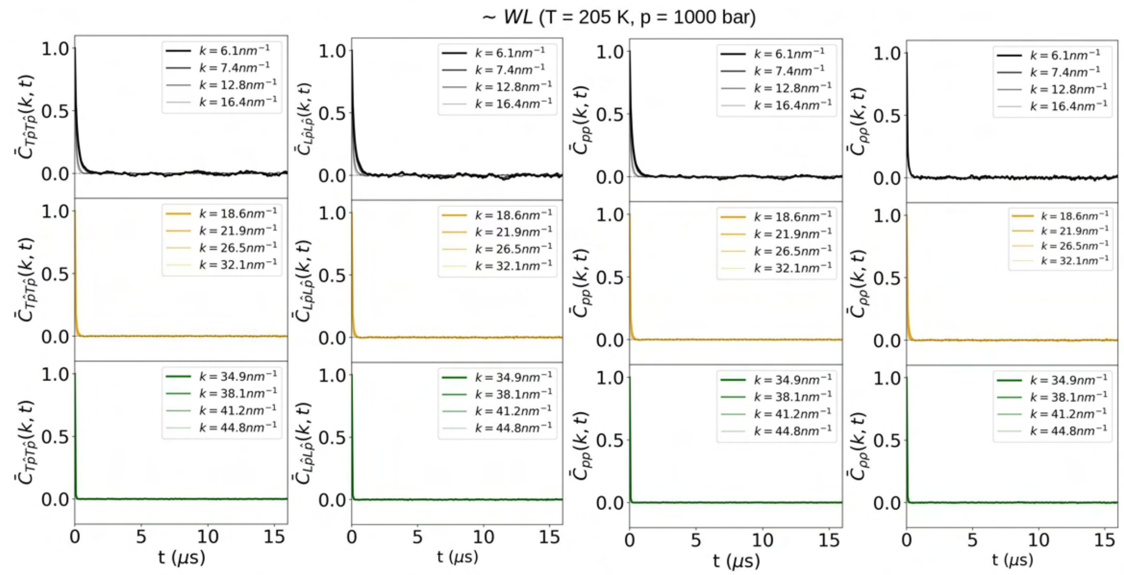

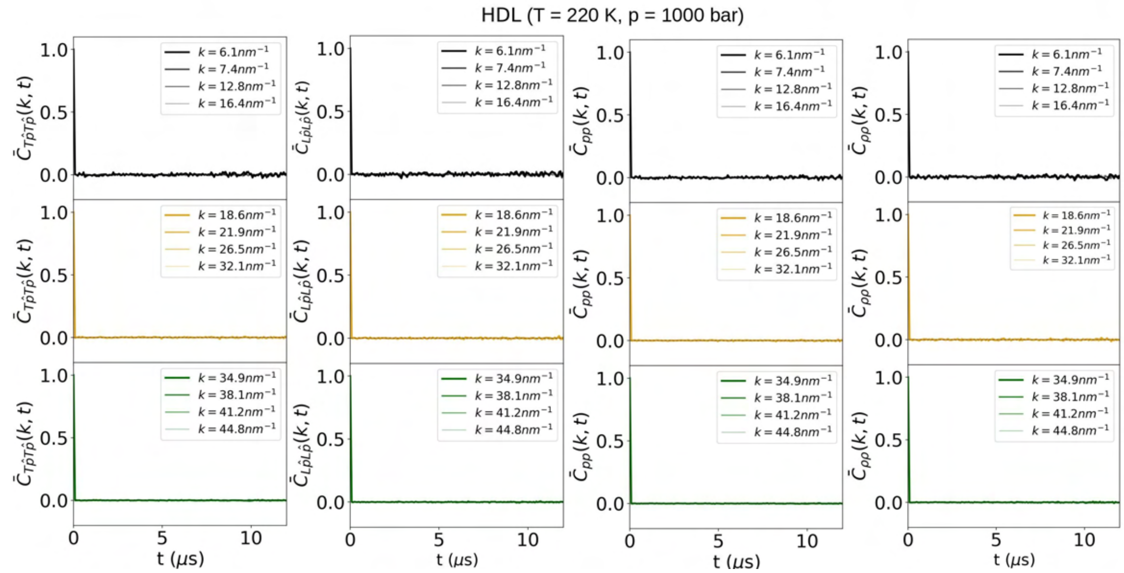

Fig. S8. Normalized $C_{T\hat{p}T\hat{p}}(k,t)$, $C_{L\hat{p}L\hat{p}}(k,t)$, $C_{PP}(k,t)$, $C_{\rho\rho}(k,t)$ at different T's along the $p = 1000$ bar isobar crossing the WL.

LDL (T = 190 K, p = 0 bar)

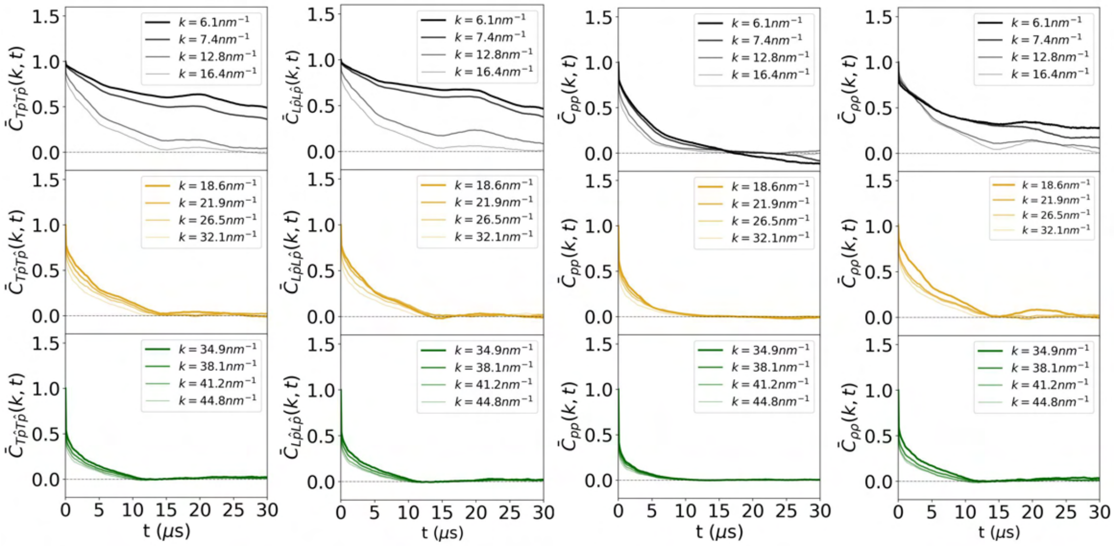

LDL (T = 196 K, p = 0 bar)

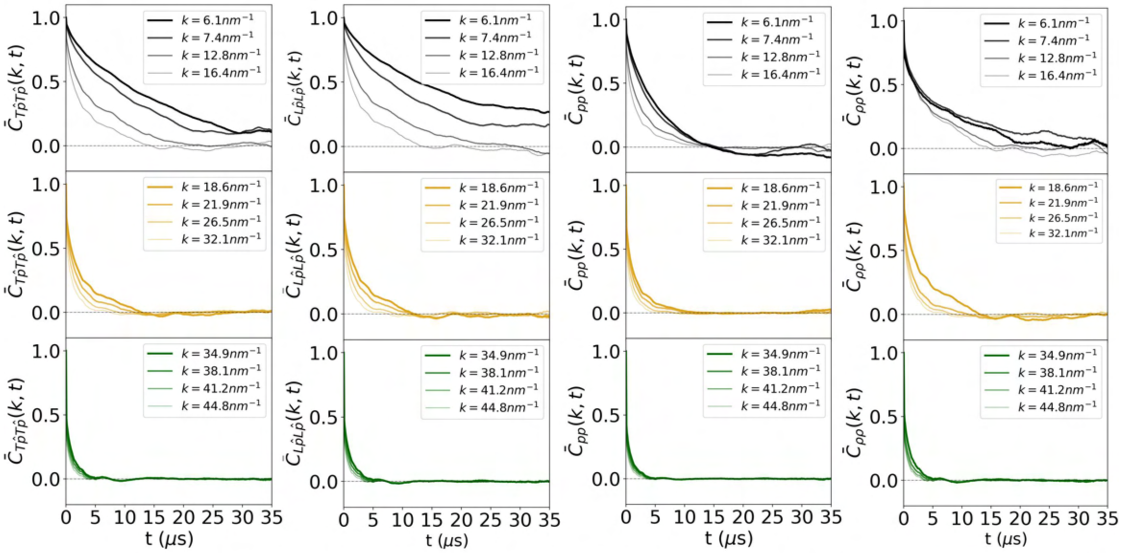

$\sim$ *WL* (T = 205 K, p = 0 bar)

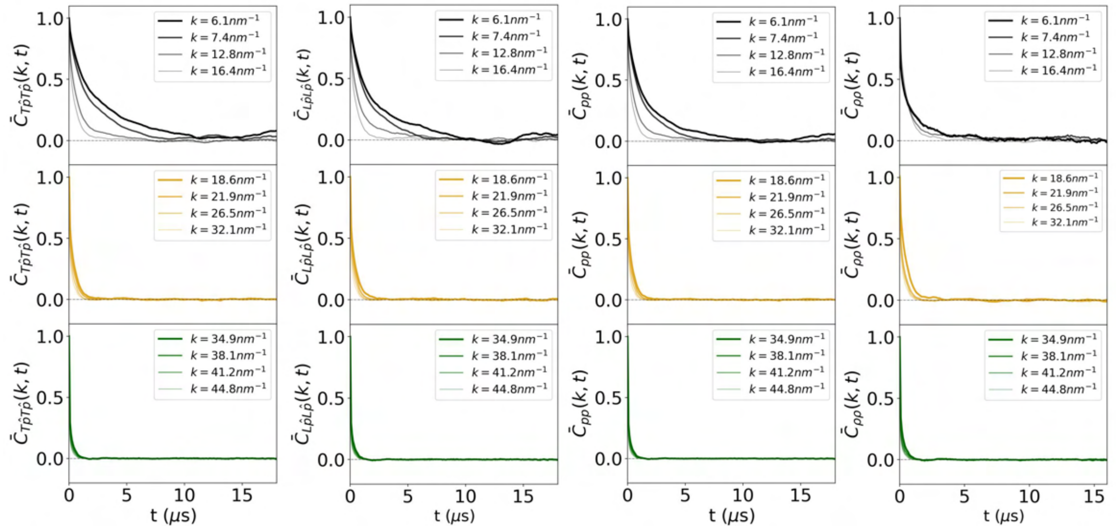

Fig. S9. Normalized $C_{T\hat{p}T\hat{p}}(k,t)$, $C_{L\hat{p}L\hat{p}}(k,t)$, $C_{PP}(k,t)$, $C_{\rho\rho}(k,t)$ at different T's along the $p = 0$ bar isobar, crossing the WL.

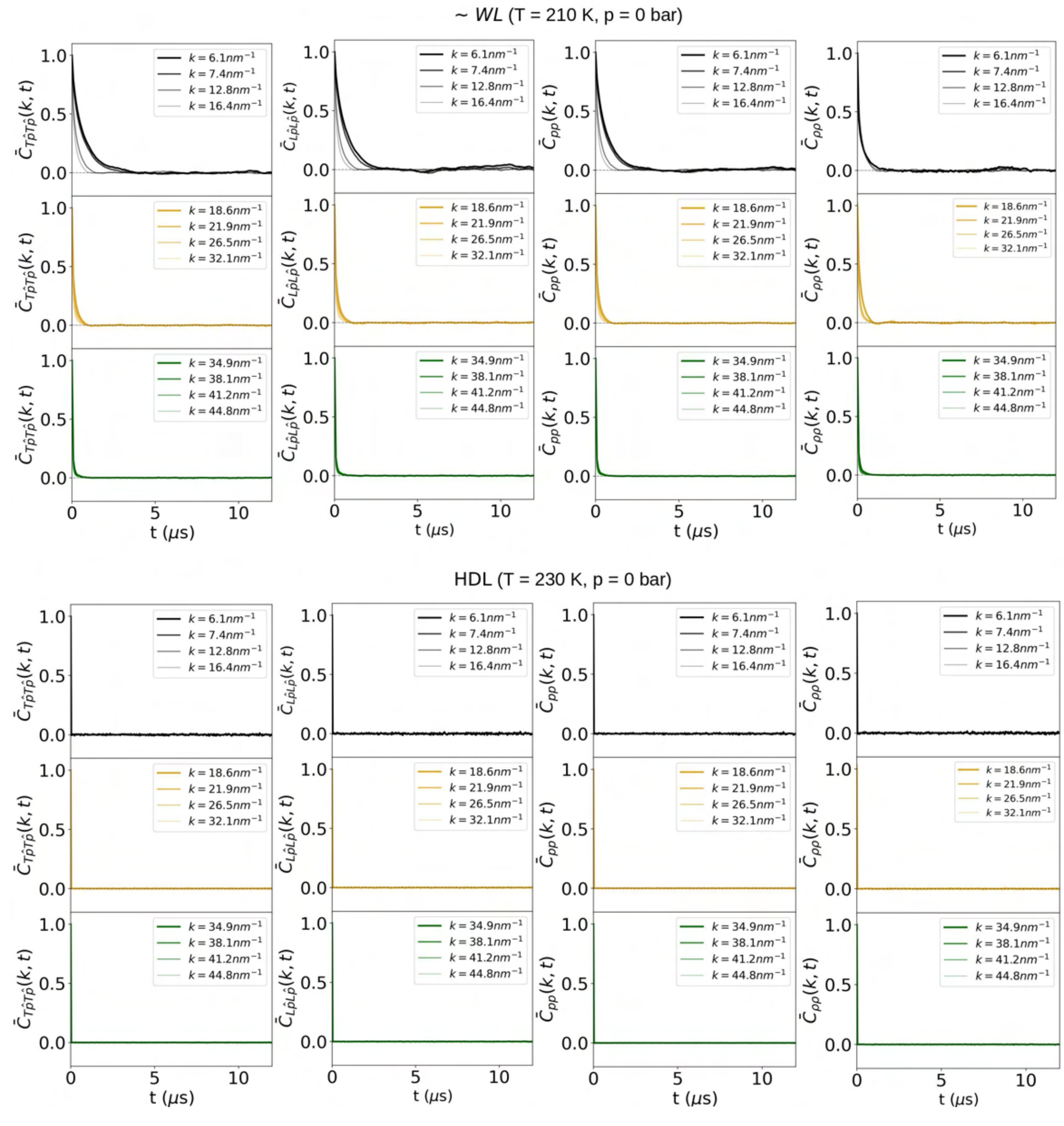

Fig. S10. Normalized $C_{T\hat{p}T\hat{p}}(k,t)$, $C_{L\hat{p}L\hat{p}}(k,t)$, $C_{PP}(k,t)$, $C_{\rho\rho}(k,t)$ at different T's along the $p = 0$ bar isobar, crossing the WL.

LDL (T = 170 K, p = 2500 bar)

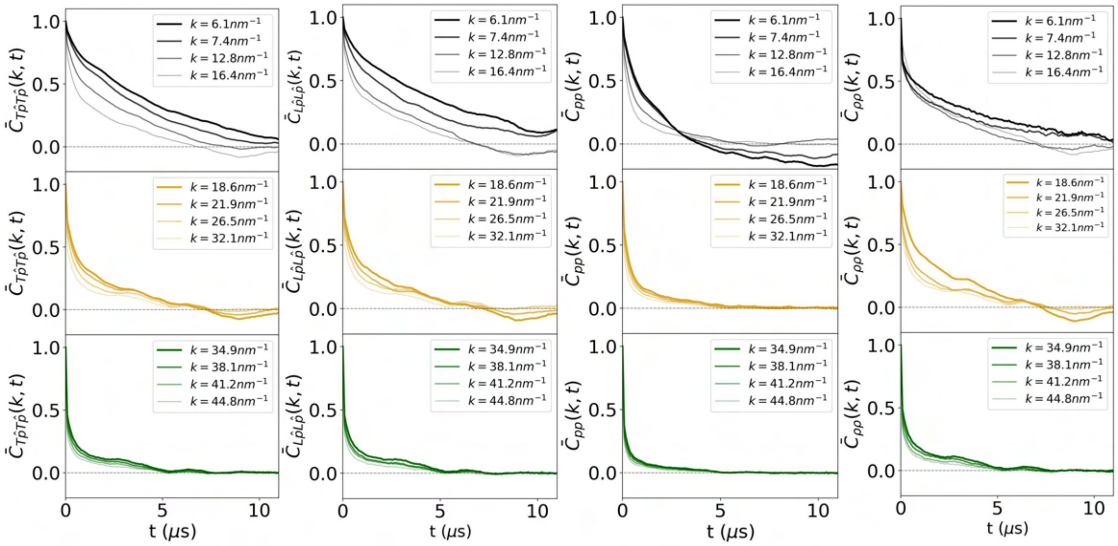

HDL (T = 180 K, p = 2500 bar)

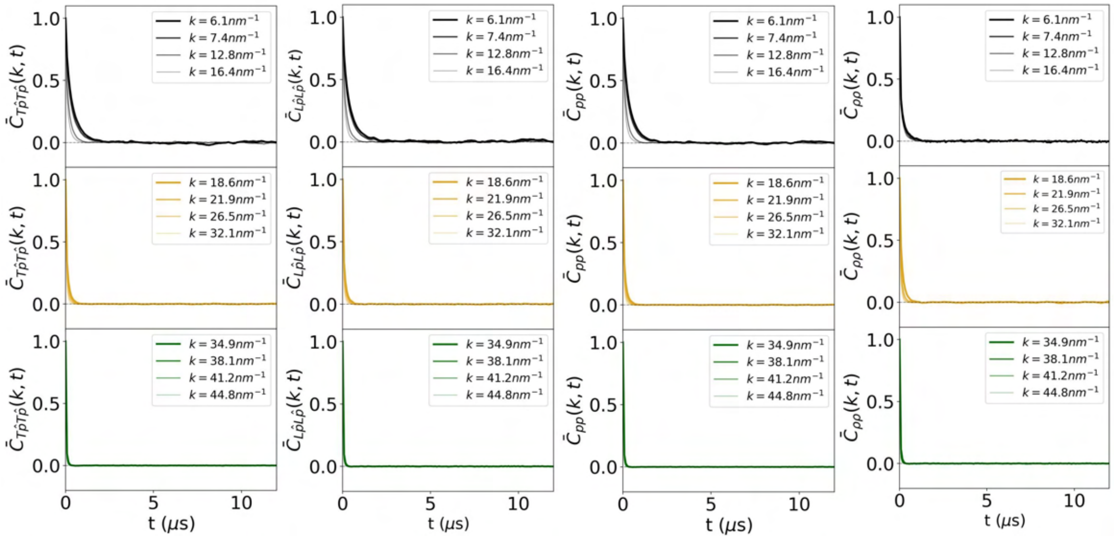

Fig. S11. Normalized $C_{T\hat{p}T\hat{p}}(k,t)$, $C_{L\hat{p}L\hat{p}}(k,t)$, $C_{PP}(k,t)$, $C_{\rho\rho}(k,t)$ at different T's along the $p = 2500$ bar isobar, crossing the first-order LLPT line.

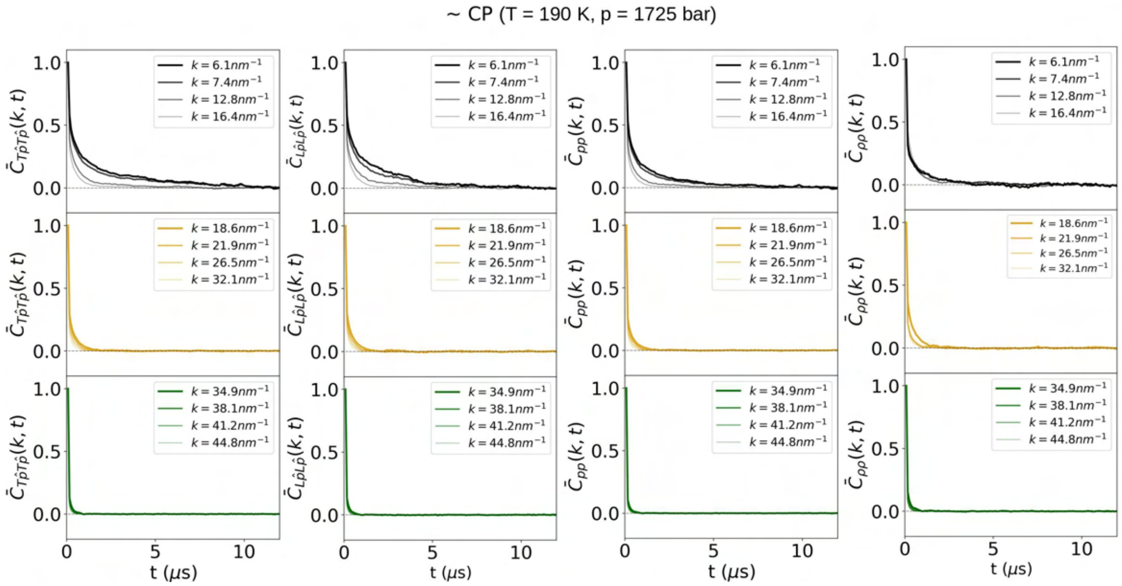

Fig. S12. Normalized $C_{T\hat{p}T\hat{p}}(k,t)$, $C_{L\hat{p}L\hat{p}}(k,t)$, $C_{PP}(k,t)$, $C_{\rho\rho}(k,t)$ at CP.

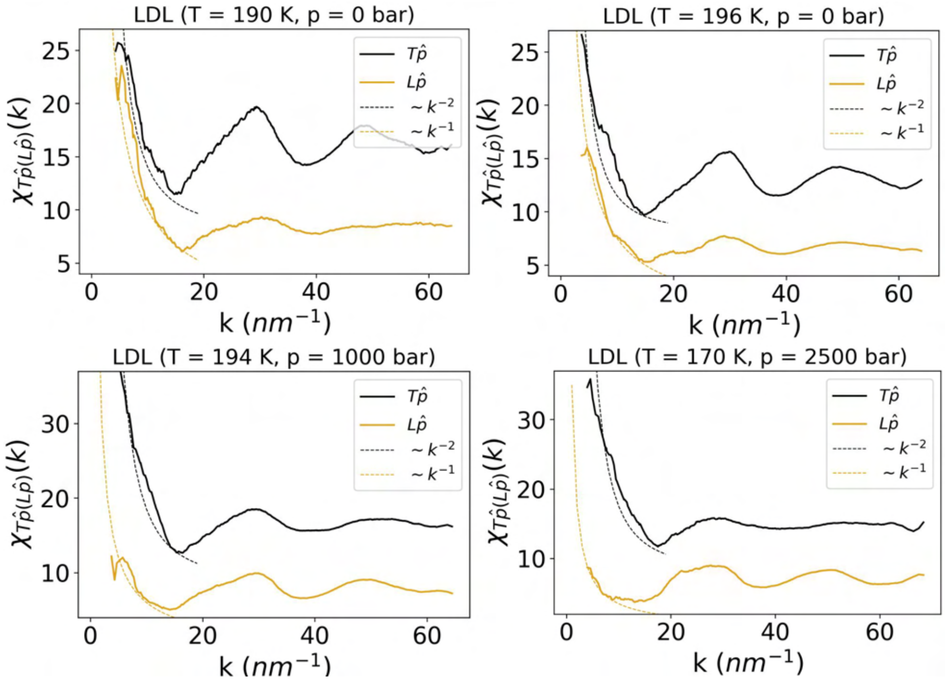

Fig. S13. Static susceptibilities $\chi_{T\hat{p}(L\hat{p})}(k)$, in LDL in different points of the (p, T) plane as a function of k.

References

1. PG Debenedetti, F Sciortino, GH Zerze, Second critical point in two realistic models of water. *Science* **369**, 289–292 (2020).
2. M Matsumoto, T Yagasaki, , H Tanaka, Chiral ordering in supercooled liquid water and amorphous ice. *Phys. Rev. Lett* **115**, 197801 (2015).
3. OV Dolgov, DA Kirzhnits, EG Maksimov, On an admissible sign of the static dielectric function of matter. *Rev. Mod. Phys.* **53**, 81–94 (1981).
4. PA Bopp, KA A., G Sutmann, Frequency and wave-vector dependent dielectric function of water: Collective modes and relaxation spectra. *J. Chem. Phys.* **109**, 1939 (1998).
5. D Forster, *Hydrodynamic fluctuations, broken symmatry, and correlation functions.* (The Benjamin/Cumings publishing company), (1975).
6. A Patashinskii, V Pokrovskii, *Fluctuation Theory of Phase Transitions.* (Pergamon Press), (1979).
7. P Tang, R Iguchi, K Uchida, GEW Bauer, Excitations of the ferroelectric order. *Phys. Rev. B* **106**, L081105 (2022).
8. A Widom, S Sivasubramanian, C Vittoria, S Yoon, YN Srivastava, Resonance damping in ferromagnets and ferroelectrics. *Phys. Rev. B* **81**, 212402 (2010).
9. JP Hansen, McDonald, *Theory of Simple Liquids.* (4th edition. Academic Press, London), (1990).
10. JP Boon, S Yip, *Molecular Hydrodynamics.* (Dover Publications, Inc., New York), (1991).
11. C Fox, A generalization of the cauchy principal value. *Can. J. Math.* **9**, 110–117 (1957).
12. MG Izzo, G Ruocco, S Cazzato, The mixing of polarizations in the acoustic excitation of disordered media with local isotropy. *Front. Phys.* **6**, 108 (2018).